Limitations to the validity of single wake superposition in wind farm yield assessment

Limitations to the validity of single wake superposition in wind farm yield assessment

K. Gunn[1], C. Stock-Williams[1], M. Burke[1], R. Willden[2], C. Vogel[2], W, Hunter[2], T. Stallard[3], N. Robinson[4], S. R. Schmidt[5]

[1]Uniper Engineering, Technology Centre, Ratcliffe on Soar, Nottingham, NG11 OEE, UK
[2]Department of Engineering Science, University of Oxford, OX1 3PJ, UK
[3]School of Mechanical, Aerospace and Civil Engineering, University of Manchester, Manchester, M13 9PL, UK
[4]AWS TruePower, 463 New Karner Road, Albany, NY 12205, USA
[5]E.ON Climate & Renewables, Carl Gustafs väg 1, SE-205 09 Malmö, Sweden

Kester.Gunn@uniper.energy

Abstract Commercially available wind yield assessment models rely on superposition of wakes calculated for isolated single turbines. These methods of wake simulation fail to account for emergent flow physics that may affect the behaviour of multiple turbines and their wakes and therefore wind farm yield predictions. In this paper wake-wake interaction is modelled computationally (CFD) and physically (in a hydraulic flume) to investigate physical causes of discrepancies between analytical modelling and simulations or measurements. Three effects, currently neglected in commercial models, are identified as being of importance: 1) when turbines are directly aligned, the combined wake is shortened relative to the single turbine wake; 2) when wakes are adjacent, each will be lengthened due to reduced mixing; and 3) the pressure field of downstream turbines can move and modify wakes flowing close to them.

1. Introduction

Commercially available wind farm energy yield assessment models rely on superposition of wakes calculated for isolated single wind turbines [1,2,3,4]. This is generally achieved through linear summation of momentum [5] or energy [6] deficits, although some models simply take the largest of the wake deficits present at any given point in space [1,2]. These methods of wake simulation fail to account for emergent flow physics that may affect the behaviour of multiple turbines and wakes and therefore farm yield predictions. This study investigates whether single wake superposition methods may contribute to any systematic errors in yield estimates; and whether commercial wind farm energy yield modelling software requires more explicit modelling of wake interactions. This study builds on that of Machefaux et al [7] by presenting the physical causes of discrepancies between analytical modelling and simulations or measurements.

2. Approach

2.1. Turbine Layouts

Several layouts of two turbines (126m diameter 5MW NREL reference turbine [8]) have been investigated through cross-comparisons of analytical models with numerical simulations (computational fluid dynamics, “CFD”). Additional model scale flume experiments (“tank tests”) are

also presented to provide comparison for several layouts. These turbine layouts, shown in Fig. 1, have been chosen to investigate the fundamental assumptions in single turbine superposition models:

1. overlapping wakes (i.e. when the inflow to the wake-generating turbines is undisturbed); and
2. interacting wakes (i.e. when the inflow to at least one of the turbines is partly or wholly in the wake of another).

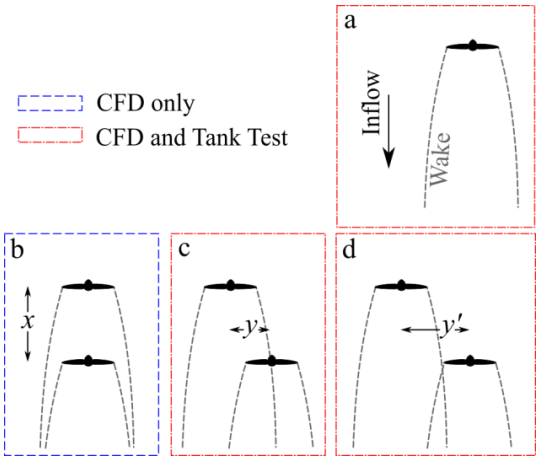

Figure 1. Summary of experimental investigations carried out with CFD and tank testing. CFD parameters at full scale are x=8D, y=1D, y'=1.75D, D=126m. Tank test parameters are x=4D, y=1D, y'=1.4D, D=0.27m.

2.2. CFD Simulations

The CFD was performed using ANSYS Fluent 15.0, solving the steady 3D incompressible Reynolds Averaged Navier-Stokes (RANS) equations using the finite volume method [9]. An embedded Blade Element actuator method was used to represent the rotors in this study, resulting in free shear emanating from the edges of the rotor disks, while avoiding the need to compute the shear caused by the rotor blade surfaces. Zero equation turbulence models, such as the Baldwin–Lomax model, calculate the eddy viscosity based on the local boundary layer profile at walls, and are therefore not well suited to actuator type simulations. Turbulence closure is therefore provided through the two-equation k-ω SST model [10], which combines the advantages of the k-ω with the k-ε turbulence closures near no-slip boundaries and through the remainder of the domain respectively; leading to it having been employed in a number of previous wind turbine studies (e.g. [11,12]). While the turbulence model is known to have an influence on the quantitative development of wake profiles, the qualitative trends presented herein are generally valid. A shear profile was generated by introducing a constant shear stress to the bottom wall of the computational domain, which results in velocity shear and a turbulence profile across the rotor height. The shear stress was adjusted to achieve a hub height turbulence intensity of around 5%.

The blades of the 126m diameter three-bladed rotor have sections varying smoothly between the DU40 and DU21 sections from 20% to 70% of the blade radius, and then the NACA64-series section out to the blade tip. The root chord is 4.6m and tapers to 1.4m at the tip. The blades are twisted through 13.1 degrees between root and tip [8]. The rotor was simulated using a RANS embedded Blade Element actuator disk model, with lift, drag and swirl injected at approximately 7000 points over each of the rotor disks in response to the simulated local flow-field [13]. Unlike analytic Blade Element Momentum methods, azimuthal averaging is not required and the effect of the shear on rotor loading and wake generation can be simulated through the embedded actuator disk.

Active torque control was implemented for the rotors, allowing the angular speed of each rotor to be independently varied. Following M. O. L. Hansen [14], the angular speed was adjusted to match the

aerodynamic torque, $T_{aero} = P/\omega$, with the generator torque, $T_{gen} = K\omega^2$, where K (the "mode gain") is a property of the turbine that was determined from single rotor simulations in which ω was adjusted to achieve the peak power coefficient. The active torque control algorithm therefore ensured that the angular speed of each rotor was adjusted to achieve operation at maximum power coefficient. Rotor hubs, ellipsoids of length 1/10th of the rotor diameter, and with a radius of 1.5m, were modelled in each case but support towers were neglected. The key simulation parameters are given in Table 1.

Table 1. Summary of CFD parameters

Bulk flow wind speed	12.0 m/s
Hub height wind speed (u_0)	11.4 m/s
Hub height turbulent kinetic energy	0.538 m^2/s^2
Hub height turbulence intensity	5.26%
Domain width	1134 m
Domain length	3150 m
Domain height	1134 m
Number of cells	6-8 x 10^6
Rotor diameter	126 m
Rotor hub height	90 m

2.3. Tank tests

The tank tests were conducted in the University of Manchester wide flume with key dimensions as given in Table 2. Three-bladed rotors were employed with blade section selected for high lift to drag ratio at a chord Reynolds number of approximately 3×10^4 (typical at three-quarter radius) and with radial variation of chord length and twist selected to produce typical variation of thrust with tip speed ratio. Rotor thrust was measured through a strain-gauged supporting structure and power from rotor angular speed, measured by digital encoder, multiplied by torque supplied by a DC motor with friction subtracted. Torque was selected for equal tip speed ratio of each rotor. Flow velocity was measured with a Nortek Vectrino+ sampling at 200 Hz. The flow characteristics, rotor and instrumentation are described further by T. Stallard et al [15]. With reference to Fig. 1, the upstream rotor was located at the flume mid-span and mid-depth, 22 diameters from the inflow and the downstream rotor at x=4D, y'=1.4D. Transects of velocity were taken at hub height at 2D increments downstream.

Table 2. Summary of tank test parameters

Hub height flow speed	0.463 m/s
Hub height turbulence intensity	12%
Tank width	5 m
Length of test section	12 m
Still water depth	0.45 m
Turbine diameter	0.27 m
Turbine hub height	0.225 m

2.4. Wake combination methods

The three wake combination methods most often used in the literature are given in Eqns. 1 to 3, where $u_{norm,i}$ are the wakes at that location, from each upstream turbine i in isolation. Note that these combination methods take the effective normalisation speed for each turbine to be that turbine's inflow speed, not the free stream speed. Results from the use of these methods are presented for comparison with the CFD and tank tests (colour lines in Figs. 4 – 7).

Largest deficit: $$U_{norm} = \min\left(u_{norm,1}, u_{norm,2}, \dots\right) \quad (1)$$

Root-sum-square: $$U_{norm} = 1 - \sqrt{\sum \left(1 - u_{norm,i}\right)^2} \quad (2)$$

Linear: $$U_{norm} = 1 - \sum \left(1 - u_{norm,i}\right) \quad (3)$$

3. Results and Analysis

Rotor wake data are now presented. The origin of the domain is at the centre of the upstream rotor. To account for the shear profile, velocities are normalised relative to the value at the corresponding cross-stream (y) and vertical (z) position at the furthest upstream plane of the domain, i.e.

$$u_{norm} = \mathrm{u}(x, y, z) \,/ \mathrm{u}(-4, y, z)$$

where all distances are normalised to the rotor diameter D.

3.1. Single Turbine Analysis

In order to establish a baseline for comparison with multiple turbine data, the single turbine wake is first examined. Fig. 2a (far left column) illustrates that the location of largest velocity deficit behind a turbine shifts with downstream distance:

1. to the right, due to the swirl injected by the rotor; and
2. towards the ground, due to the velocity shear driving re-energisation of the wake region more strongly above than below the wake.

This wake evolution is not represented in commercial analytical wake models, although it does appear in Fuga simulations (a linearised CFD model) [4]. This indicates that hub height velocity may not be the most appropriate choice of measurement to characterise the wake [16].

Otherwise, as shown further in Fig. 3, the Gaussian shaped wake profile is seen in the far wake, as expected from many previous studies [17].

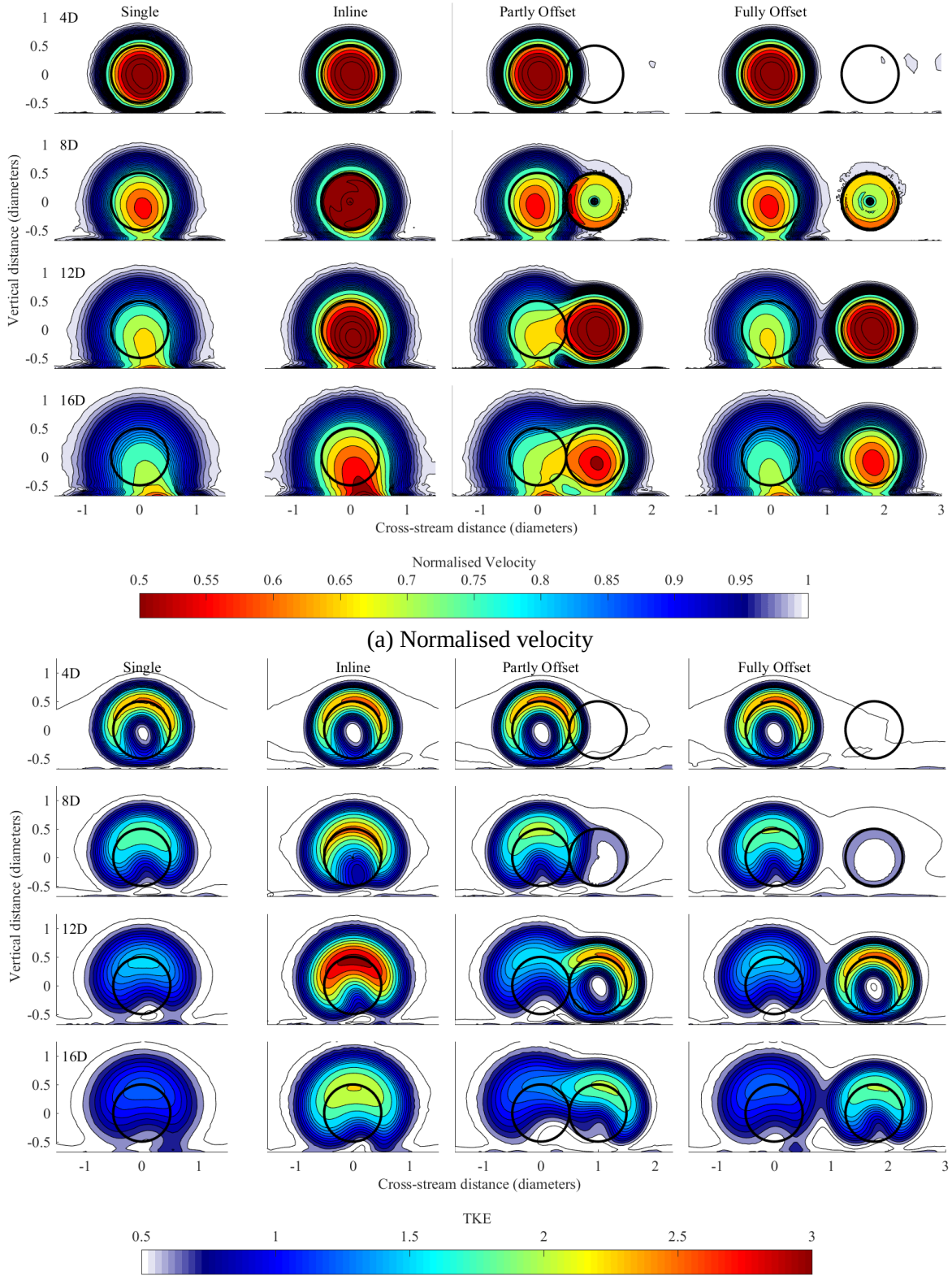

(a) Normalised velocity

(b) Turbulent kinetic energy, TKE

Figure 2. Normalised velocity (a) and turbulent kinetic energy (b) distribution over vertical planes downstream of each rotor. Downstream position is relative to the upstream rotor. The colours indicate contours, where white is the colour of the undisturbed value. The rotor areas are marked as black outlines. (CFD simulation)

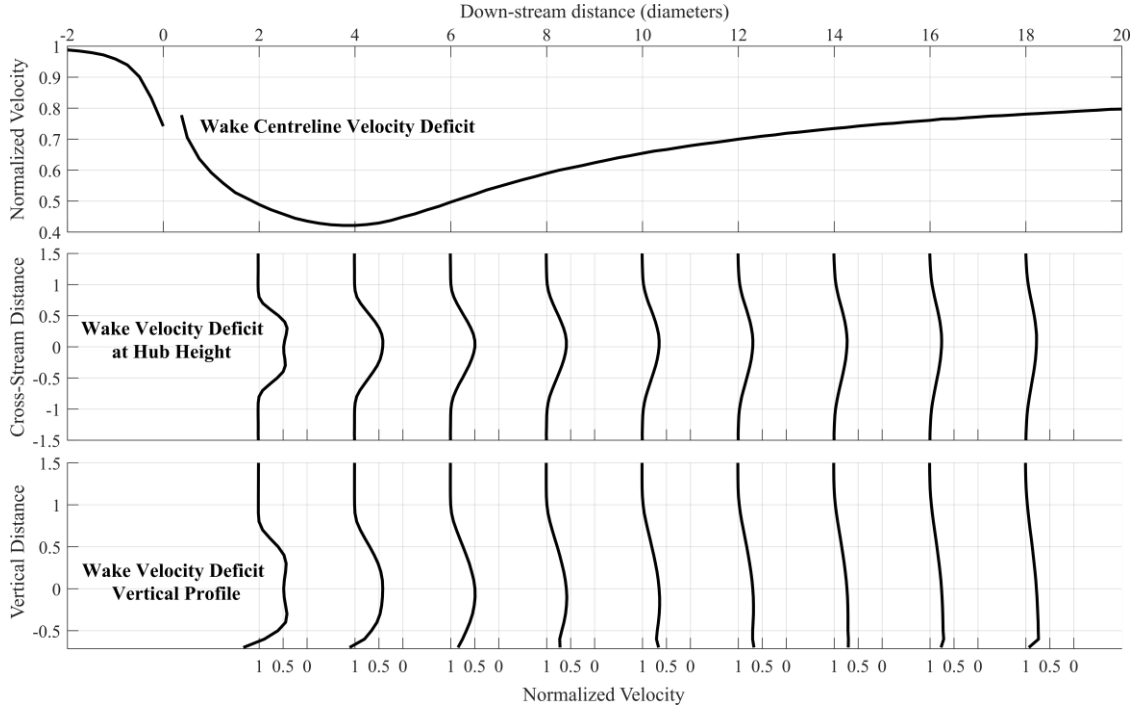

Figure 3. Normalised velocity profiles behind a single turbine (CFD simulation).

3.2. Two Turbine Analysis

Table 3 gives an overview of rotor performance from the CFD simulations.

Table 3. Summary of rotor performance. Power coefficient (C_P) and thrust coefficient (C_T) are calculated relative to the flow speed 2.5D upstream of each hub (u_i). Power and thrust of each turbine also shown relative to the single turbine case (P_0 and T_0 respectively).

Case	C_P	P/P_0	C_T	T/T_0	u_i/u_0
Single Rotor	0.536	1	0.914	1	1
Inline					
- Upstream Rotor	0.532	0.999	0.904	0.999	1
- Downstream Rotor	0.507	0.284	0.859	0.424	0.668
Partly Offset					
- Upstream Rotor	0.532	0.999	0.904	0.999	1
- Downstream Rotor	0.590	0.932	0.968	0.953	0.944
Fully Offset					
- Upstream Rotor	0.532	1.000	0.904	0.999	1
- Downstream Rotor	0.544	1.022	0.917	1.014	0.997

3.2.1. Inline Rotors. The most studied turbine configuration is the case of a downstream turbine fully contained within another's wake [18,19,20,21]. The key result from several studies of real and simulated turbines is that the flow speed recovers faster behind two turbines than behind one turbine, resulting in a third turbine - placed directly in line with the first two turbines at the same spacing - producing more power than the second turbine. This effect is shown clearly in Fig. 7 of Gaumond et al. [21].

This is also reproduced by the CFD results. Referring to Fig. 2a and comparing the single rotor cases at 4D and 8D (left-most column, top two plots) with the same distances behind the second rotor in the inline case (i.e. 12D and 16D, second-left column, lowest two plots), the wake deficit is only marginally greater. Table 2 indicates that thrust, and hence rate of momentum extraction, by the downstream turbine is lower than for an isolated turbine and thus a marginally smaller deficit is expected. The subsequent rate of wake recovery is also higher and this is explained by the higher value of turbulence observed downstream of the second rotor (Fig. 2b).

Fig. 4 further illustrates this effect and shows how the different wake combination methods perform for this case at 16D downstream of the upstream rotor. The two grey dashed lines show the individual wakes observed for the stated downstream distance for each rotor if assumed to operate in isolation. The combined wake from the CFD is shown in black. The centreline velocity deficit behind the two rotors is marginally smaller than the case for the isolated wake 8D downstream of the second turbine. The downstream turbine operates at significantly lower thrust (42.4%) and thus momentum removal than the upstream or isolated turbine, and hence the deficit is reduced relative to the isolated case. The three wake combination methods applied to the independent wakes are shown as coloured lines. It is clear that none exactly match the actual combined wake (i.e. the black line).

This demonstrates why the largest or "worst" velocity deficit (red line in Fig. 4) is used by WindFarmer and OpenWind to combine wakes together [1,2]: this method results in the best agreement in validation studies (in which cases are selected carefully, e.g. by widening or narrowing the direction sector - and hence range of onset flow angles - within which data is considered [21]). Figs. 5-7 will illustrate that this is not the case when a line of rotors is not directly aligned with the flow direction.

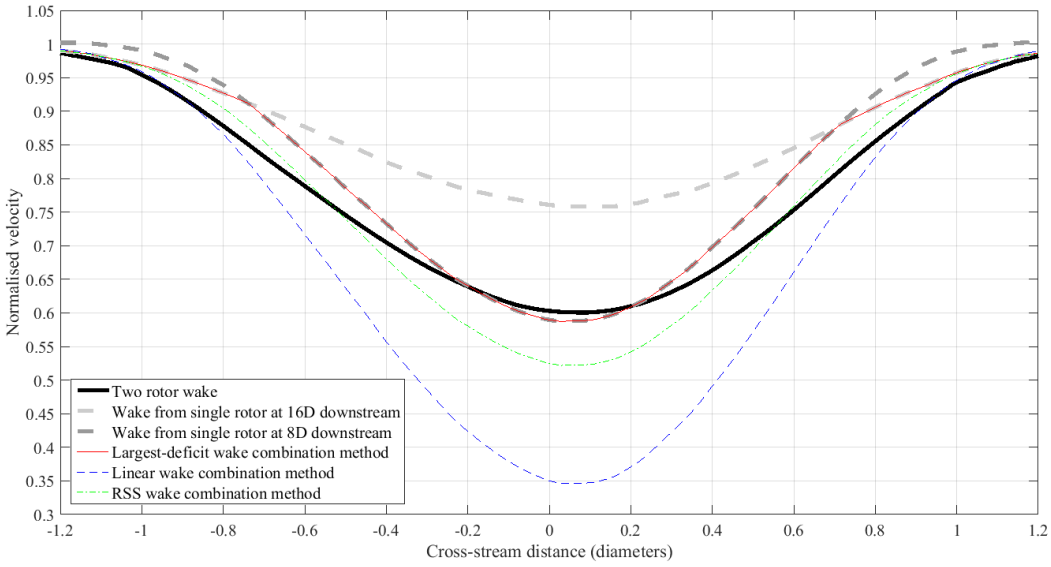

Figure 4. Normalised hub-height velocity profiles behind two in-line rotors, at 16D behind the first (8D behind the second) (black). Also shown are the wakes from the two rotors operating independently (thick lines, grey). Finally different combination methods, applied to the independent wakes, are shown (thin lines, colour). (CFD simulation).

Semi-empirical wake models could be altered to describe the enhanced recovery in the fully in-line case more accurately by using a variable near wake length model, such as that proposed by Sørensen et al [22].

3.2.2. Partly Offset Rotors. As can be seen in Table 3, the inflow to the second turbine in this case has been reduced, with a corresponding reduction in power for that turbine (93% of the single rotor). Further, as is clear from Fig. 2a, at 8D downstream of first turbine the onset flow to the second turbine is sheared horizontally (with a 21.6% difference in velocity across the rotor diameter). Fig. 5 demonstrates that the unphysical largest-deficit approach does not perform well when the swept area of the downstream rotor is only partly exposed to the wake of the upstream turbine. Indeed, the simulated effect of the two rotors is a much greater wake deficit over most of the width of the wake profile. It is postulated that this is because there is less energy available between the two wakes, resulting in recovery occurring over a longer distance as the energy must be obtained from the flow above and on either side of the aggregate wake (see Fig. 2a, second-from-right column).

A further deviation from the assumptions of commercial wake models can be observed in Fig. 2b for this configuration (second-from-right column). The TKE distribution in the downstream rotor wake is asymmetric (planes at 8D, 12D and 16D). This differs from the nearly symmetric distribution of the isolated rotor simulation, which more closely matches the standard eddy-viscosity wake models.

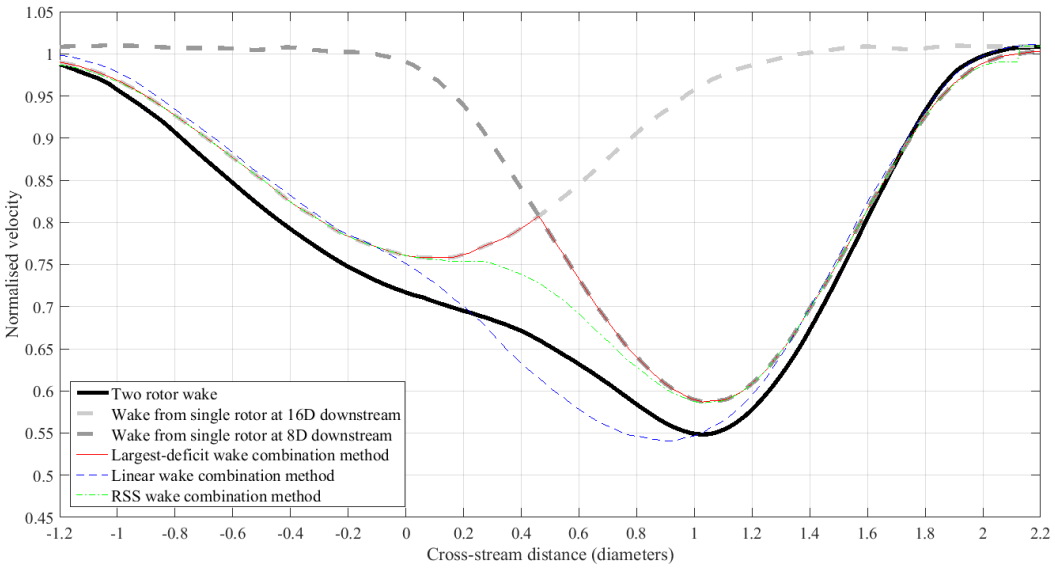

Figure 5. Normalised hub-height velocity profiles behind two partly offset rotors. Lines as described in Fig. 4 (CFD simulation).

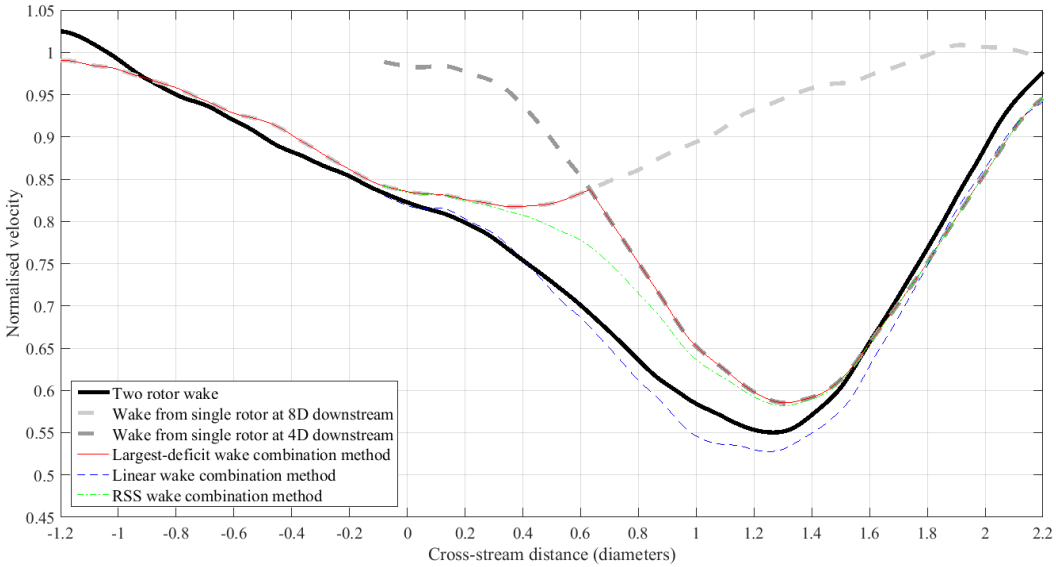

Figure 6. Normalised hub-height velocity profiles behind two partly offset rotors, at 8D behind the first (4D behind the second) (black). Also shown are the wakes from the two rotors operating independently (thick lines, grey). Finally different combination methods, applied to the independent wakes, are shown (thin lines, colour). (tank tests).

The effect is corroborated by the velocity measurements from the tank tests, as shown in Fig. 6 for the same configuration (except with a streamwise turbine separation of 4D rather than 8D, used due to the more rapid wake expansion associated with higher ambient turbulence of the tank tests).

This situation of rotors partly exposed to the wake of turbines located upwind occurs rather commonly in practice, so modification to the standard approach of superposition of single-wake models should be considered to enable better prediction of average energy yield over the life of a wind farm. If the direction sector in energy yield validation studies is chosen to be sufficiently wide (depending on the turbine layout) to average over both partly and fully in-line cases, this may result in such models providing improved long-term performance and behaving in a consistent manner when turbine positions are gradually altered for layout optimisation.

3.2.3. Fully Offset Rotors

In the fully offset case, the second rotor's wake - both velocity deficit and turbulence (right-hand columns of Figs. 2a and 2b respectively) - are only slightly altered from the single rotor case, since the two wakes do not interact strongly.

However, this case also demonstrates interesting physics. Fig. 7 shows that the upstream rotor's wake has been offset by approximately D/8, due to the pressure field created by the downstream rotor. Compared with the partly offset or fully in-line cases, the wake due to two fully offset rotors cannot therefore be expressed as a simple combination of single symmetric rotor wakes. This effect is further shown in Figs. 8 and 9.

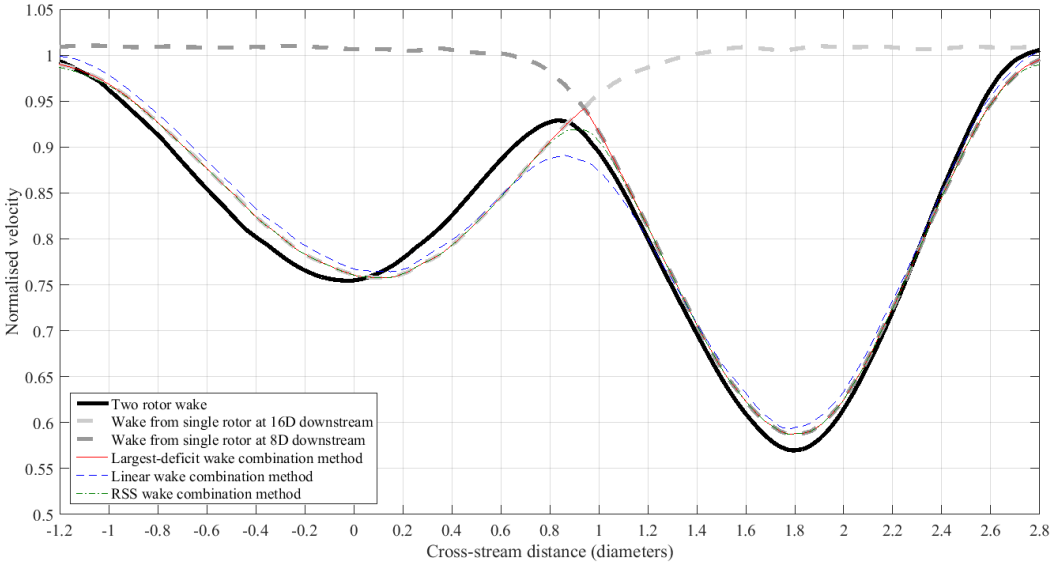

Figure 7. Normalised hub-height velocity profiles at 16D behind two fully offset rotors. Lines as described in Fig. 4 (CFD simulation).

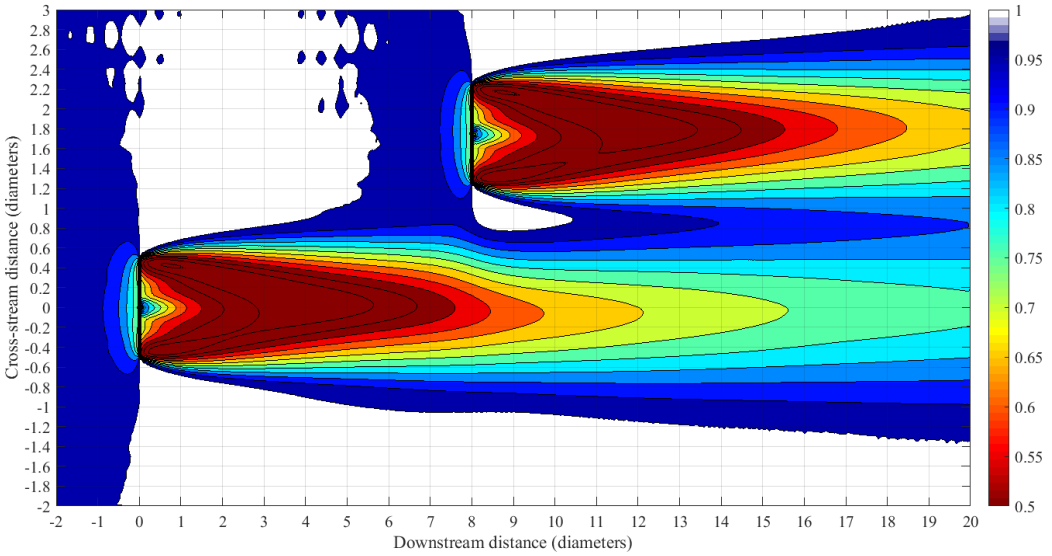

Figure 8. Map of normalised streamwise velocity at hub height for two fully offset rotors, flow incident from the left (CFD simulation).

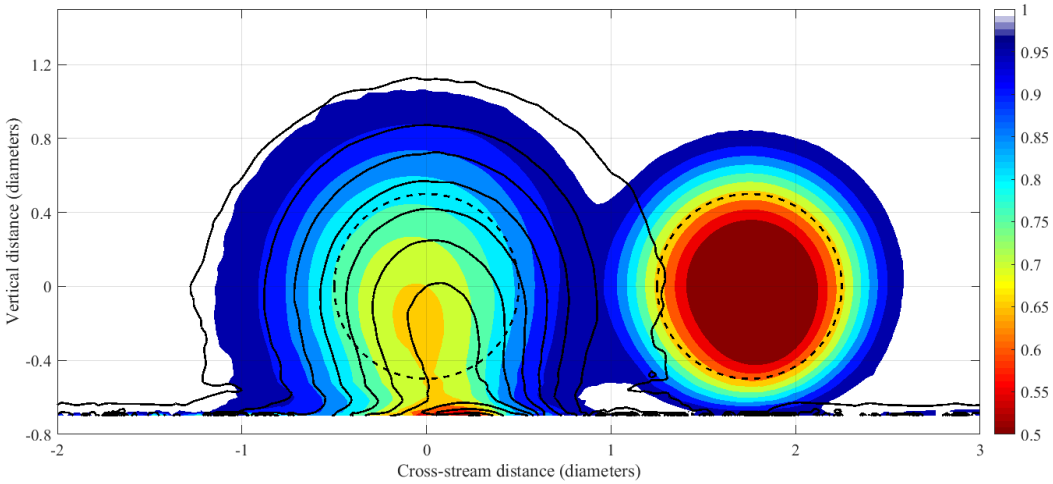

Figure 9. Normalised velocity cross-section at 12D downstream of the first of two fully offset turbines (coloured contours). The rotor areas are marked as black dashed outlines. The solid black contours indicate the locations of same velocity contours in the single turbine case, demonstrating how the upstream turbine's wake has been shifted and squeezed in the cross-stream direction (CFD simulation).

4. Conclusions

Investigations of configurations of one and two full-scale wind turbine rotors using CFD simulations, and corroborated by experiment, have shown that wake combination methods currently used in commercially available software for calculation of energy yield from wind farms neglect important aspects of the flow physics. The rate of wake recovery and rotor performance have been investigated for two rotors with the downstream rotor aligned with, partially offset and fully offset from the upstream rotor to assess typical configurations occurring within a wind farm during operation. Various wake model validation studies, typically concentrating on wind flow closely aligned with the axis of a row of turbines, have been previously used to justify a largest-deficit approach to combining individual wakes from semi-empirical or analytic models. However, this study has shown that, when the swept area of the downstream turbine is not fully enclosed in the wake of the upstream turbine, a much deeper wake deficit is produced than calculated for the same turbine in isolation, entailing significant over prediction of velocity of the two turbine wake for the largest-deficit and RSS combination approaches. Hence power output of turbines located downstream would be over predicted. When turbines are located just outside the wake of upstream turbines, this study has demonstrated emergent flow physics, particularly that the pressure field generated by the downstream rotor shifts the upstream wake laterally and compresses it.

These effects indicate that consideration should be given to implementing more than simplistic combination of pre-solved single turbine wakes when simulating wind farms for energy yield, particularly for the cases of partly offset wakes. An option would be to solve the flow equations of the Eddy Viscosity model developed by Ainslie, but with explicit consideration of the presence of upstream and nearby turbines.

A significant factor in the rate of deficit recovery is the turbulence of the surrounding flow. Improved agreement may be obtained if wake models accounted for onset wake turbulence for the in-line case, and for asymmetry between the adjacent wake turbulence and ambient turbulence for the offset wake

configurations. A general approach could be to characterise the azimuthal variation of turbulence around the wake.

References

[1] AWS Truepower 2010 *OpenWind Theoretical Basis and Validation*

[2] DNV GL. 2011 *WindFarmer Theory Manual*

[3] EMD International 2011 *WindPRO Introduction to Wind Turbine Wake Modelling and Wake Generated Turbulence*

[4] Ott S, Berg J, Nielsen M. 2011 *Linearised CFD Models for Wakes*

[5] Jensen N O 1983 A Note on Wind Generator Interaction

[6] Ainslie J F 1988 Calculating the Flowfield in the Wake of Wind Turbines *J. Wind Eng. Ind. Aerodyn.*

[7] Machefaux E, Larsen G C and Murcia Leon J P 2015 Engineering models for merging wakes in wind farm optimization applications. *JPCS*.

[8] Jonkman J, Butterfield S, Musial W and Scott G 2009 *Definition of a 5-MW Reference Wind Turbine for Offshore System Development.*

[9] ANSYS Inc. 2013 *ANSYS Fluent 15.0 Theory Guide*.

[10] Menter F R 1994 Two-equation eddy-viscosity turbulence models for engineering applications. *AIAA J.* **32**

[11] Sørensen N M, Michelsen J A and Schreck S. 2002 Navier-Stokes predictions of the NREL phase VI rotor in the NASA Ames 80-by-120 wind tunnel. *In 2002 ASME wind energy symposium.* VA: American Institute of Aeronautics & Astronautics

[12] Mahu R and Popescu F 2011 NREL Phase VI rotor modeling and simulation using ANSYS Fluent 12.1. *Mathematical Modeling in Civil Engineering*

[13] Sanderse B, van der Pijl S P and Koren B 2011 Review of computational fluid dynamics for wind turbine wake aerodynamics. *Wind Energy*

[14] Hansen M O L. 2008 *Aerodynamics of Wind Turbines*, Second Edition London: Earthscan.

[15] Stallard T, Feng T and Stansby P K 2015 Experimental study of the mean wake of a tidal stream rotor in a shallow turbulent flow *J. Fluids Struct*

[16] Wagner R, Cañadillas B, Clifton A and Wagenaar J W 2014 Rotor equivalent wind speed for power curve measurement – comparative exercise for IEA Wind Annex 32 *JPCS*

[17] Vermeer L J, Sørensen J N and Crespo A 2003 Wind turbine wake aerodynamics. *Progress in Aerospace Sciences*

[18] Nygaard N G 2014 Wakes in very large wind farms and the effect of neighbouring wind farms *JPCS*

[19] Porté-Agel F, Wu YT and Chen CH 2013 A Numerical Study of the Effects of Wind Direction on Turbine Wakes and Power Losses in a Large Wind Farm *Energies*

[20] Westerhellweg A, Cañadillas B, Kinder F and Neumann T. 2012 Wake measurements at alpha ventus - dependency on stability and turbulence intensity

[21] Gaumond M, Réthoré P E, Bechmann A, Ott S, Larsen G C, Peña A, et al. 2012 Benchmarking of wind turbine wake models in large offshore wind farms. In Torque 2012

[22] Sørensen J N, Mikkelsen R, Sarmast S, Ivanell S and Henningson D 2014 Determination of Wind Turbine Near-Wake Length Based on Stability Analysis *JPCS*